Aerial image based mask defect detection in dense array structures

Roderick Köhle[a], Mario Hennig[b], Rainer Pforr[b], Karsten Bubke[c], Martin Szcyrba[c], Arndt C. Dürr[c]

[a] Infineon Technologies AG, Balanstr. 73, Munich, Germany;
[b] Infineon Technologies SC300 GmbH & Co. OHG, Dresden, Germany
[c] Advanced Mask Technology Center, Dresden, Germany

ABSTRACT

For leading mask technologies the mask inspection for finding critical defects is always a difficult task. With the introduction of chrome-less, high-transmission and alternating mask types, new absorber material and the possibility of quartz defects the defect inspection and -classification becomes even more challenging. To decide whether a defect is critical or a repair is successful, the Zeiss AIMS tool is used to classify defects. For conventional imaging the optical settings are usually chosen such that resolution is maximized, for example a dipole illumination is used for imaging a dense line-space array at an optimum contrast. In this paper we will do the opposite and reduce the optical resolution, such that we can filter out the array pattern and study the resulting defect image. This technique allows using a simple threshold detector to find and classify defects.

Keywords: Defect classification, Mask inspection, AIMS metrology, lithography simulation

1. INTRODUCTION

The AIMS aerial image measurement tool by Zeiss proved to be very valuable for defect review of repaired sites on the mask. The advantage of an aerial image, measured at same or similar conditions to the scanner settings of resist exposure it that it can be expected that very small distortions do not have a significant effect on the final waver print. While for arbitrary structures this analysis is straightforward as usually the defect position is identified by the context of the surrounding patterns, it turns out to be much harder to find a small defect in a repetitive environment like a dense line-space array. A solution to this problem is to automatically classify defects by comparing the measured image with a reference. While it is possible to compute a defect image by subtracting measurement by reference, it is tempting to use the optical system of the aerial image measurement system to determine the defect image by optical filtering.

1.1. Array Resolution Enhancement

For the imaging of dense array gratings, there exist two classes of resolution enhancement techniques. The first class uses an off-axis illumination to shift the diffraction orders of the mask such that the image is created by a two-beam interference [1, 2]. A second enhancement technique is the technique of alternating phase shifting masks [3]. A two-beam interference is constructed by periodically repeating the structure with alternating phases. For dipole illumination, the nominal condition for dipole illumination is given by

$$\sigma_{center} = \frac{\lambda}{2P \cdot NA}, \sigma_{radius} \leq 1 - \sigma_{center}, \quad (1)$$

where

λ, NA : wavelength and numerical aperture

σ_{center} : Dipole off-axis illumination angle

σ_{radius} : Dipole aperture radius of illuminator

For alternating PSM circular illumination is used. For maximum contrast the illumination pupil must be enclosed by

$$\sigma_{circular} \le 1 - \frac{\lambda}{2P \cdot NA}. \qquad (2)$$

For off-axis illumination, the most commonly used blank transmission is 6% attenuated PSM blanks. Recently, other transmissions raised interest or are under investigation [4]. The image contrast is a function of the blank transmission and the absorber linewidth as shown in Figure 1. For any mask transmission, there are two contrast peaks. For our investigation, we choose the linewidth so that the positive contrast is maximized.

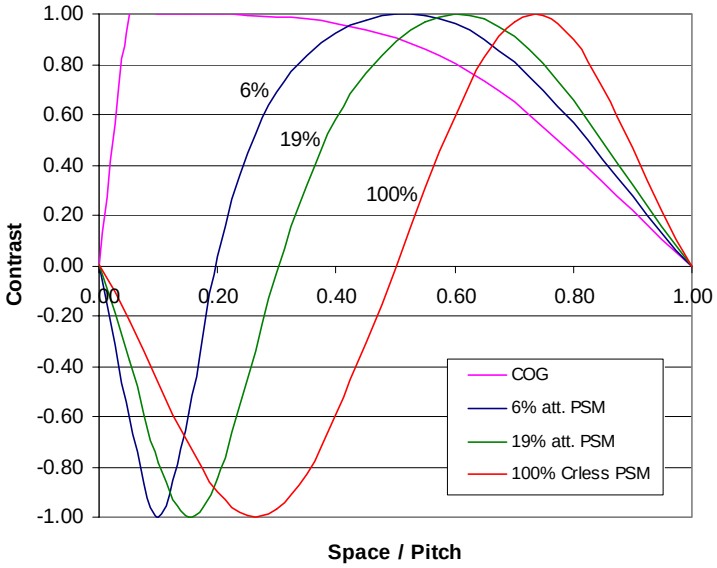

Figure 1. Contrast curves calculated for blank transmission values of 6%, 19% and 100% (Crless) PSM.

1.2. Array Resolution Suppression

From the same consideration one can derive a condition to blank out the dense array from the aerial image. However, instead of a dipole off-axis illumination a conventional centered circular illumination is used. The complementary illumination condition for the maximum sigma to obtain a defect image is given by

$$\sigma_{circular} \le \frac{\lambda}{P \cdot NA} - 1 \ . \qquad (3)$$

For alternating phase shifting masks, we use dipole illumination for measuring the defect image. The off-axis center sigma is the same as in the dipole relation of Eq. (1), whereas the radius of the dipole must satisfy Eq. (2).

If we image this array with circular illumination, we want to calculate the constant intensity level of the aerial image, since only the 0^{th} diffraction order contributes to the image, the intensity is given by

$$I_0 = \left(s + a \cdot l\right)^2 = \left(s(1+a) - a\right)^2 \qquad (4)$$

where

s : duty cycle of space, s=space/pitch

l : duty cycle of line, l=line/pitch

a : absorber field transmission (square root of the intensity transmission).

Similarly, we can compute the constant intensity level for an alternating line-space grating. Due to the dipole illumination, only the first diffraction order is contributing to the image. The intensity level is therefore given by

$$I_1 = \left(\frac{2}{\pi}\sin\left(\frac{\pi}{2}s\right)\right)^2 = \left(\frac{2}{\pi}\right)^2 \frac{1}{2}\left(1+\sin(\pi s)\right), \tag{5}$$

where *s* is the shifter width normalized by the pitch.

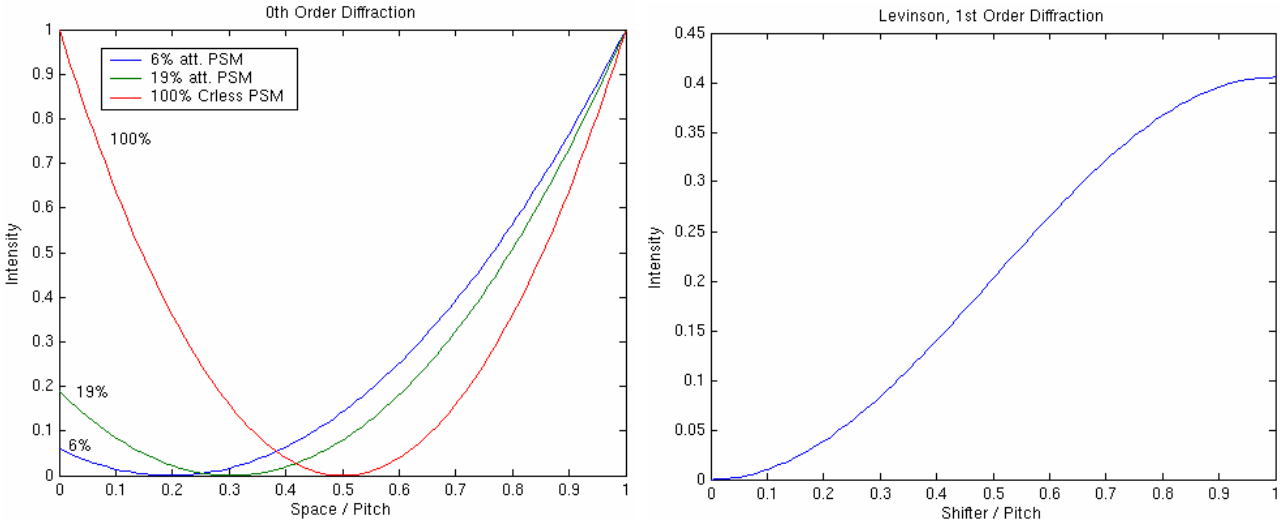

Figure 2. Intensity level of 0th order diffraction for an off-axis, attenuated PSM (left) and 1st order diffraction of a Levinson type alternating PSM (right).

Transmission $t=a^2$	Space/Pitch	Intensity level
0%	50%	0.25
6%	50%	0.14
19%	60%	0.20
100%	75%	0.23
Alt. PSM	50%	0.20

Table 1. Constant aerial image intensity levels for interesting mask types and transmission values.

One interesting aspect of this methology is that we can relate the line-width specification and the aerial image. A reasonable approach and actually a requirement for defect detection is to request that the line-width uniformity is no worse than defect image. If the defect image is within the intensity variation calculated from line-width specification, we can conclude that the defect is not critical. For the discussion here, we will assume a 2.5nm tolerancing for the mask CD line-widths.

2. SIMULATION STUDIES

In this section we will establish the defect assessment criteria and determine its relation to the defect sizes. Together with the CD linewidth specification we can obtain a first estimate about the minimum defect size that can be detectable. The layout of the structures to be studied is shown in Figure 3, in case of att. PSM we will consider a dark MoSi spot on the clear space and in case of alt. PSM we will consider a quartz bridge defect in the trench. For alternating gratings the mask might expose a balancing error, meaning that one of the shifters appears darker than its neighbor.

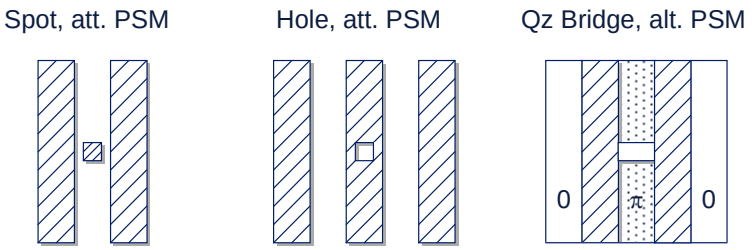

Figure 3. Defect layout of squared spot and hole defect for att. PSM and bridging defect for alt. PSM.

2.1 Defect criterion for att. PSM gratings

Figure 4 gives a first impression on the technique of using complementary illumination settings. For measuring the impact of a defect on the aerial image, we measure the change in intensity caused by the defect. In case of the image taken at nominal conditions, the defect criterion is defined as the relative defect intensity with reference to the array peak intensity. In the case of a complementary illumination, the defect criterion is defined as the relative defect intensity with reference to the background intensity.

The defect criteria derived from both imaging conditions cannot by directly compared. However, if we compute a defect thresholding level from the CD line-width specification, we have a sensitivity criterion which allows determining a minimum defect size that can be detected by the threshold from specification. In the simulation study shown in Figure 5, assuming a linewidth CD specification of 2.5%, the thresholding level becomes +/-5% for the nominal disar and +/-10% for the complementary circular illumination. From the curve plotting the relative intensity change of a defect with increasing size shows that both techniques are comparable in terms of defect sensitivity.

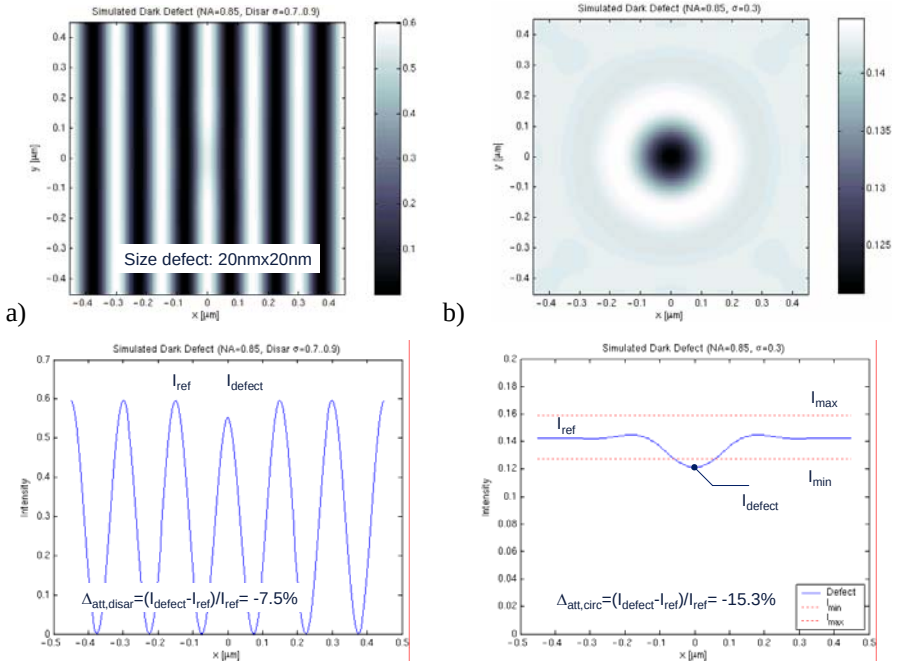

Figure 4. Image of an att. PSM spot defect of a L/S 75nm array at nominal disar (left) and complementary circular (right) illumination.

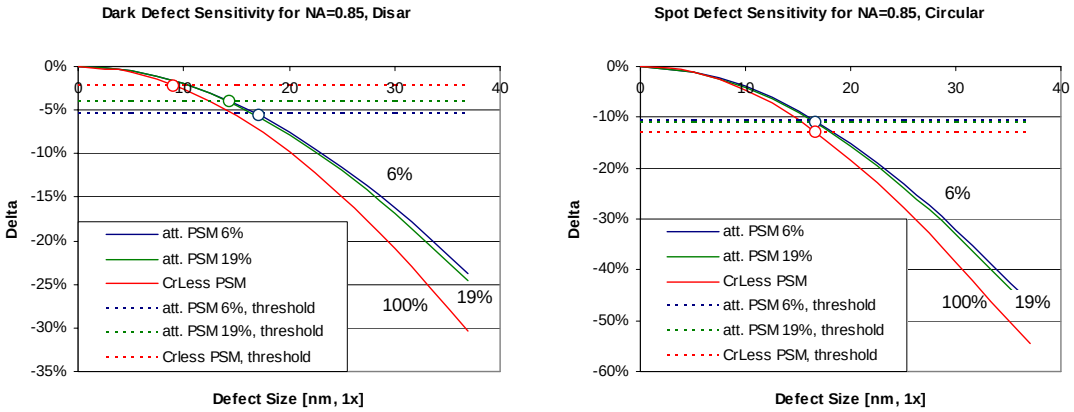

Figure 5. Defect sensitivity plot for att. PSM spot defect. (left) nominal disar illumination, (right) circular illumination. For a 2.5% mask CD specification, a minimum defect size of about 10~15nm can be tolerated for all configurations.

2.2 Defect criterion for alternating PSM gratings

For the manufacturing of alternating PSM, one well-known issue is the problem of intensity balancing [7, 8]. An ideal alternating grating must perfectly cancel out the 0^{th} diffraction order. In practice this condition can never be perfectly met so that we must assume a small asymmetry in the shifter brightness and phase. But even for a perfectly balanced mask, the change from circular to disar illumination is likely to introduce a small balancing error. To illustrate this effect, consider the simulation experiment in Figure 6. The asymmetric shifter design introduces a residual modulation at half of the array frequency.

One advantage of alternating PSM is its reduced MEEF sensitivity to symmetric CD mask errors which, however, comes at the cost of the balancing issues. Assuming the same 2.5% CD specification as for att. PSM will result in very tight intensity bounds, which are likely to be violated by balancing issues. For simplicity, we simply relaxed the CD specification to 5% to arrive at reasonable intensity thresholds of +/-10% for both illumination settings.

Figure 7 shows the defect sensitivity graph. The thresholding criteria suggest that the disar illumination might have a better defect sensitivity than using conventional circular illumination, to confirm this statement it would be required to conduct further studies regarding the influence of balancing on the defect threshold. To be able to compare the simulation results later with experimental measurements, the defect size of the bridging defects is given as the square root of defect area.

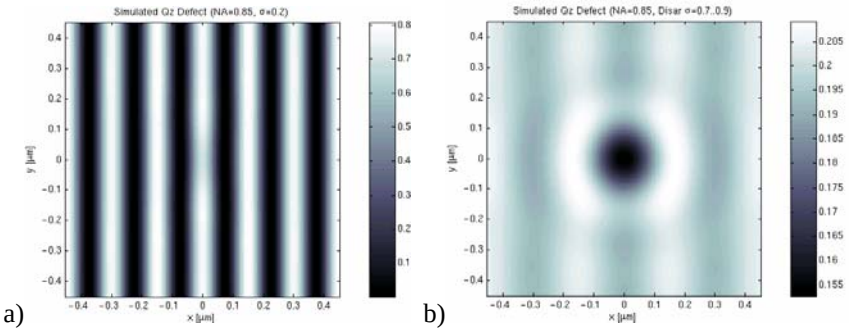

a) b)

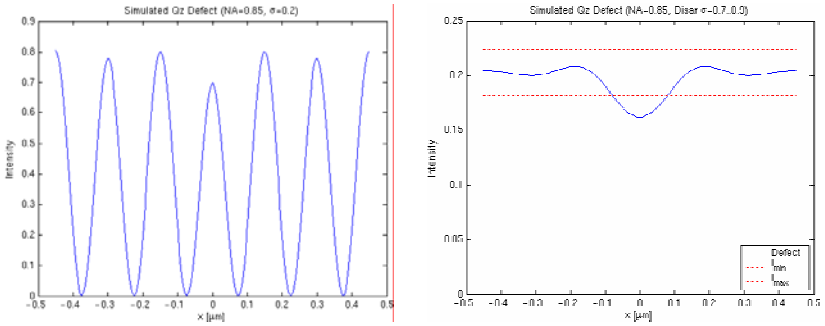

Figure 6. Effect of shifter imbalance on defect image of an alternating PSM.

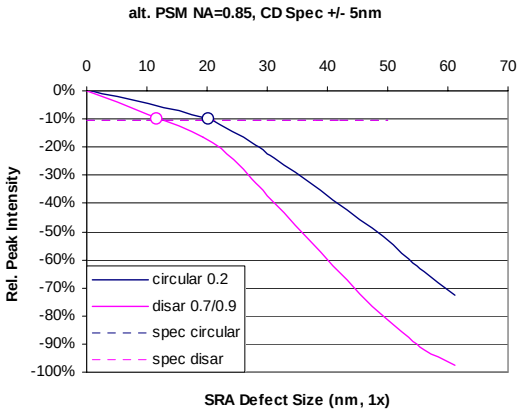

Figure 7. Defect sensitivity graph for alt. PSM Qz. Bridging defect. Threshold level corresponds to a 5nm mask CD tolerance.

3. EXPERIMENTAL RESULTS

For the experimental verification we conducted measurements using the AIMSFAB™ aerial image microscope from Zeiss [9] and by doing wafer printing experiments. The experiments allow us to assess the defect sensitivity with respect to image noise. We also conducted first printing experiments to see whether it is possible to find dark types defects, such as spots or Qz Defects, by wafer printing and inspection with an optical microscope.

3.1 AIMS measurements

To verify the applicability of the methodology described above AIMS measurements of defects were performed, using the standard settings required to print the array and settings that suppress the array leaving only the defect visible. Two types of masks were used, an alt. PSM mask with bridge-defects and an att. PSM mask with several defect types: clear, dark extensions and dark center defects. All measurements were performed on an AIMSFAB tool using 193nm as illumination wavelength and the apertures stated below. The purpose of the measurements was to investigate the limitations of the standard methodology and the method described in this paper. For each method the minimum defect size was determined at which a defect could still be detected.

To describe the way of analyzing defects the case of a dark and a clear extension on an attenuated PSM mask will be considered. Here two programmed defects in an array with a pitch of 180nm (waferscale) were investigated. The defects have lengths of 76nm and 86nm along the line of the array and widths of 20nm and 25nm (all numbers on waferscale) for the clear and the dark defect, respectively. In Figure 8 and Figure 9 the AIMS measurements of both defects are shown, using the standard setting: annular aperture with a sigma of 0.528/0.8 and a numerical aperture of 0.75. To avoid the printing of the array a circular illumination with sigma=0.4 and a numerical aperture of 0.6 was used. Shown are the full field AIMS image and a cross-section through the defect.

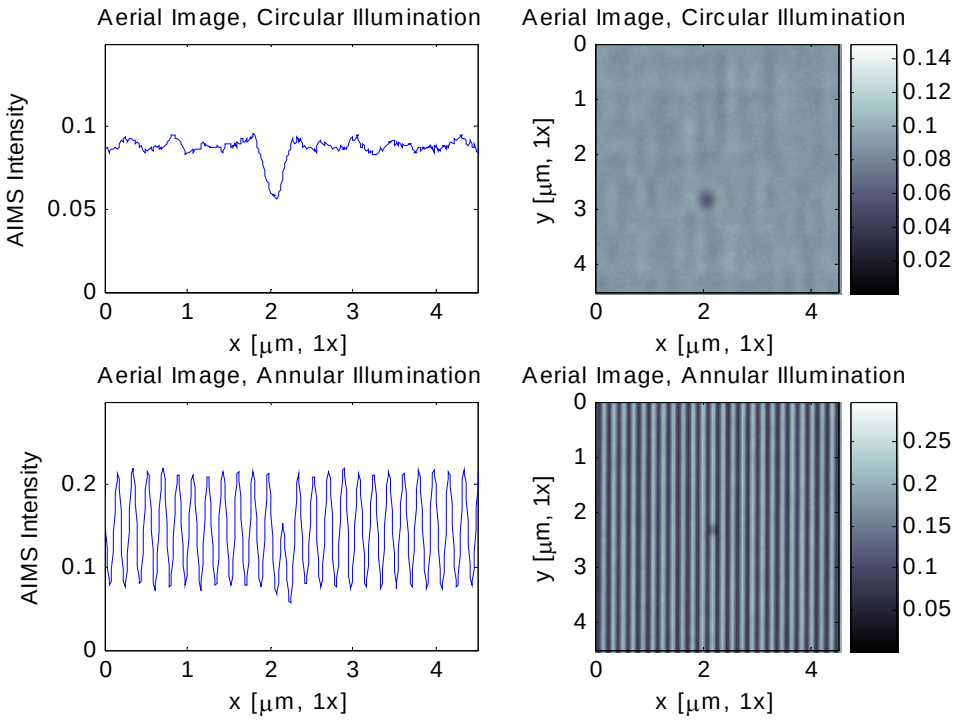

Figure 8. AIMS measurement of a clear defect using standard settings (bottom) and settings which suppress the printing of the array (top).

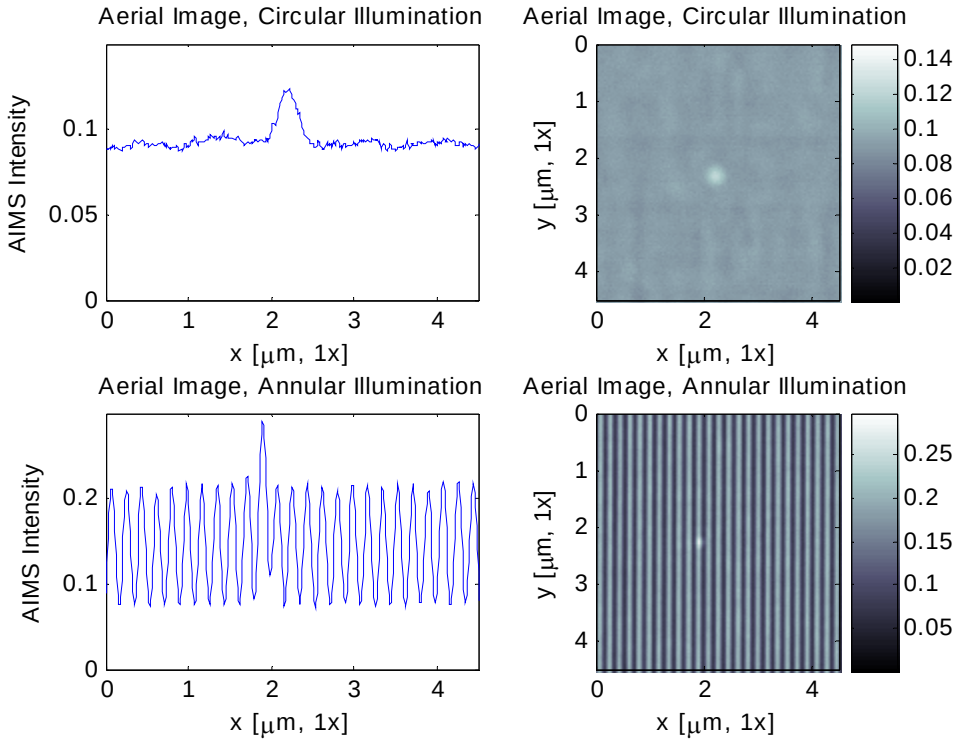

Figure 9. AIMS measurement of a dark defect using standard settings (bottom) and settings which suppress the printing of the array (top).

The defect qualification for the standard setting is performed by considering the change of the maximum and the minimum intensity at the position of the defect, $I_{\text{Defect, Max}}$ and $I_{\text{Defect, Min}}$, respectively. These values are compared to those of the defect free pattern and the following criteria can be used for the evaluation of the printability of the defect

$$\text{Max Trans} = \left(\frac{I_{\text{Defect, Max}}}{I_{\text{Defect-free, Max}}} - 1 \right) \cdot 100\% \quad \text{and} \quad \text{Min Trans} = \left(\frac{I_{\text{Defect, Min}} - I_{\text{Defect-free, Min}}}{I_{\text{Defect-free, Max}} - I_{\text{Defect-free, Min}}} \right) \cdot 100\% \, .$$

By determining values for Max Trans and Min Trans that are critical for the printing of a defect in the wafer lithography process one can classify a defect and trigger a repair process if necessary.

These criteria cannot be applied if the array is not imaged in the AIMS measurement. In this case an analogy of Max Trans can be used instead, given by

$$\text{Defect Deviation} = \left(\frac{I_{\text{Defect, Peak}}}{I_{\text{Defect-free, Average}}} - 1 \right) \cdot 100\% \, ,$$

where $I_{\text{Defect-free,Average}}$ is the (constant) intensity in the defect-free area and $I_{\text{Defect,Peak}}$ is the maximum deviation of intensity from this constant level at the defect in best focus plane. This deviation is positive for clear defects and negative for dark defects. A correlation analysis with Max Trans and Min Trans delivers the required critical values for the defect deviation to classify the printing behavior of the defect. As can be seen in the above figures the intensity is varying even in defect-free regions of the array. This is due to statistical variations in the measurement, variations of the pattern quality of the array or even systematically due to, for example, an imbalancing of an alt. PSM mask as shown below. These variations determine a detection limit for defects because only if the deviation caused by the defect is larger as the deviations in the defect-free area one can find the defect. The deviations from the predicted intensity profile in the defect-free area of the mask can be described by a 3σ value, where σ represents the standard deviation. For the standard illumination setting one can fit a sine function with a period given by the pitch of the pattern and then subtract this function from all measurement points [6]. For the setting which leads to a constant intensity level the average of all points (again, by excluding the defect and its surrounding) can be subtracted from the measurement and the 3σ value can be determined in analogy to the other case.

The residuals used to determine the 3σ value can show different behavior depending on the mask type and the mask process, namely the quality of the exposure process. As an example Figure 10 shows an AIMS measurement of a defect on an alt. PSM mask using a disar aperture for illumination. Here the residuals in the defect-free area show a sinusoidal modulation that can be related to an imbalancing of the mask.

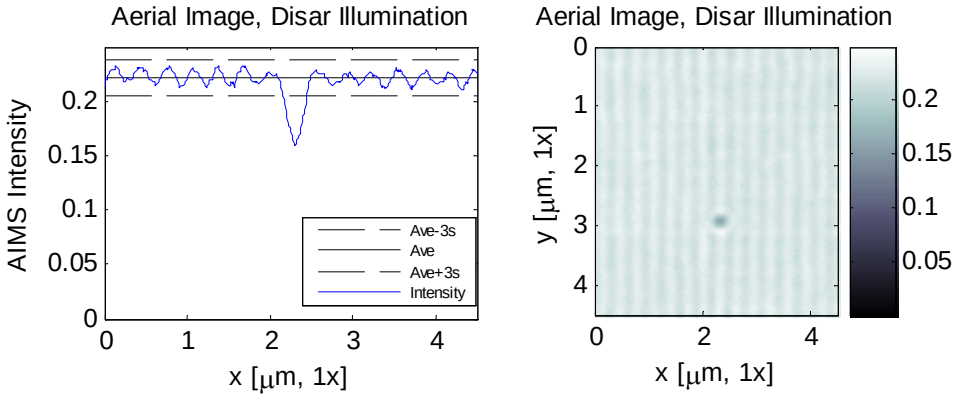

Figure 10. Intensity measurement through a dark bridging defect on an AltPSM mask.

To compare the minimum defect size that can be detected using the two methods discussed here, AIMS measurements were performed at programmed defects with varying size. The two types of defects investigated here are: bridging defects at an alt. PSM mask with a pitch of 300nm and dark defects centered in the spaces of an att. PSM mask with a

pitch of 150nm. For each defect the standard illumination settings were used and MaxTrans and MinTrans were determined on one hand, on the other side illumination settings were used that suppress the array and the defect deviation was determined. For each measurement the 3σ value of the defect-free area was calculated. The results are summarized in Table 2 and Table 3, respectively. Since the shape of defect as measured by SEM is not comparable to the ideal shape in the layout, the defect sizes are defined as the square root of the SEM defect area (SRA) [5].

	Disar Illumination (σ_{out}=0.9, σ_{in}=0.7, opening 40°, NA=0.8)		**Circular Illumination (σ=0.3,NA=0.92)**		
SRA Defect Size 1x [nm]	Defect Deviation [%]	3σ	Max Trans [%]	Min Trans [%]	3σ
50	-67.8	0.016	-51.9	-3.7	0.093
42	-56.9	0.010	-42.1	-2.6	0.089
38	-29.2	0.017	-22.3	-1.6	0.089
13	-13.7	0.011	-8.1	-0.5	0.031

Table 2. Defect Qualification criteria for bridging defects on an alt. PSM mask.

	Circular Illumination (σ=0.3, NA=0.92)		**Disar Illumination (σ_{out}=0.9, σ_{in}=0.7, opening 40°, NA=0.8)**		
SRA Defect Size 1x [nm]	Defect Deviation [%]	3σ	Max Trans [%]	Min Trans [%]	3σ
77	-89.8	0.016	-49.7	-8.2	0.044
72	-82.3	0.019	-45.5	-5.5	0.044
61	-77.6	0.017	-36.4	-6.0	0.033
54	-59.9	0.017	-28.4	-3.1	0.030
37	-29.9	0.020	-10.9	-1.1	0.044

Table 3. Defect Qualification criteria for dark center defects on a 6% att. PSM mask.

In both cases one finds that the 3σ range is higher for an illumination which images the array. This higher noise level is due to the fitting error with the array reference.

In a further step, the defect size and the defect qualification criteria can be correlated and compared to the detection limit, the 3σ value. From an extrapolation of this relation the minimum size of a detectable defect can be determined. In the left part of Figure 11 the intensity deviation after imaging with disar illumination of the defects of the alt. PSM mask is shown for different defect sizes and compared to the 3σ value and simulations of the defect deviation. The same is done for circular illumination in the right part of Figure 11. From the measurements of the alt. PSM defects one finds a minimum detection size of 5nm for the method without imaging the array and 12nm for the conventional illumination setting.

Also shown in Figure 11 are simulations of the intensity deviation at the defects. Using these simulations one finds minimum defect sizes of 10nm and 20nm for the method without array and with array, respectively. The measured defects have a much lower contrast as expected from simulation. Thus, simulations yield different values for the smallest detectable defect size. These differences can be related to effects like flare, 3d mask structure effects and other effects that were not taken into account here.

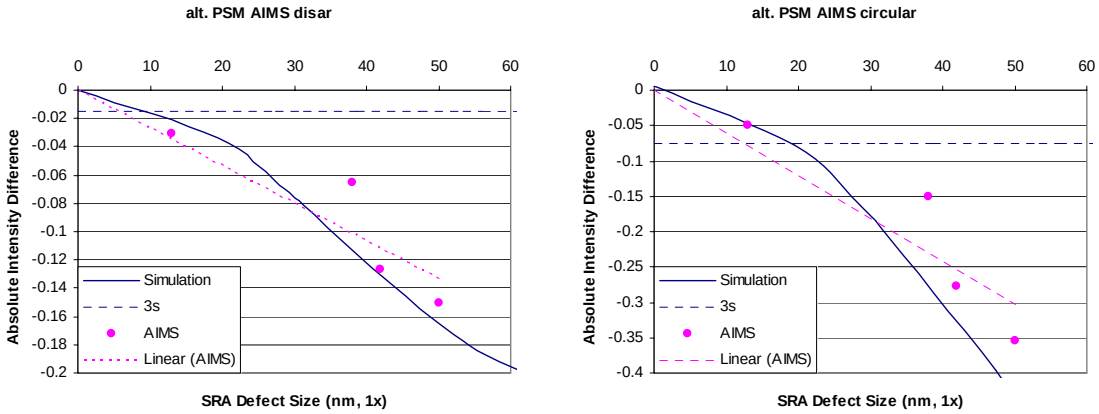

Figure 11. Deviation of intensity at defect from main pattern for alt. PSM bridging defects using disar (left) and circular (right) illumination.

In Figure 12 the same methodology is applied to defects of an att. PSM mask. In this case one finds detection limits of 17nm for circular and 24nm for disar illumination. Again, the measurements show that an illumination that suppresses the array is more sensitive and allows to find smaller defects.

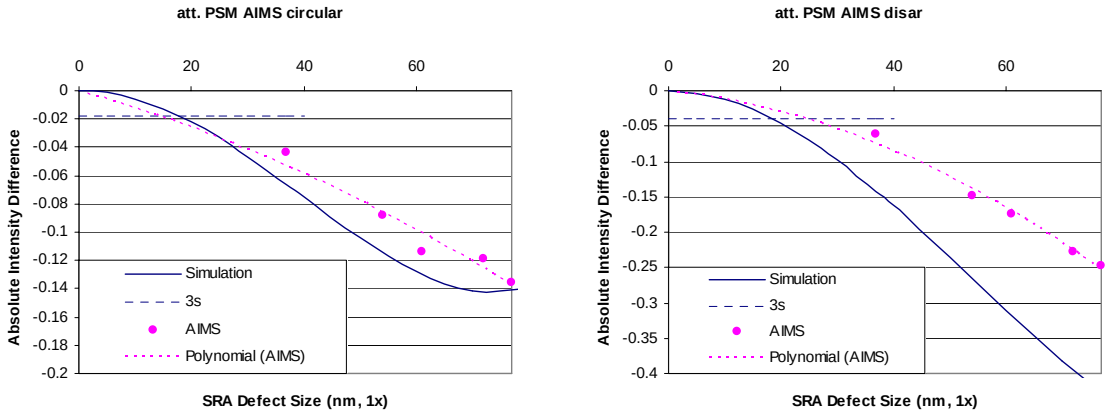

Figure 12. Deviation from main pattern of intensity at defects for 6% att. PSM dark centered defects using circular (left) and disar (right) illumination.

Both cases show that by suppressing the array one can detect smaller defects than by using the conventional illumination. The signal processing required to match the array with a reference and to compute a difference image, increases the background noise level significantly as compared to the optical filtering method.

To conclude the discussion of the measurement, it was shown that the methodology of eliminating the array by choosing appropriate illumination settings and, thus, leaving only the defect to be measured, is feasible. Indications were shown that this method is more sensitive and that it can be used to find and qualify defects which could not be found by application of conventional illumination settings. Thus, beside its use for defect qualification it can be used to verify or extend results given by inspection tools. By further analyzing the signal in the defect-free area of the mask one might be able to study other parameters related to pattern quality, like balancing of strong phase-shift masks or pattern placement quality of the array, etc. This application will not be discussed here but is left for a future investigation.

3.2 Wafer printing

For the wafer printing experiments, we were considering the alternating testmask only. The exposure at disar illumination was done at about twice the dose used for standard circular illumination. Interestingly, the remaining wafer

dots were visible by using a wafer microscope using darkfield settings. A comparison between the wafer microscope image and defect map from mask inspection is shown in Figure 13. Comparing the microscope image with the mask KLA inspection, most but not all defects are visible. A defect printing example for defects in an alternating array is shown in Figure 14. The defect sizes are the same as the ones shown in Table 2. By adjusting dose and defocus, it is possible to also print the smallest mask defect of an SRA size of 13nm.

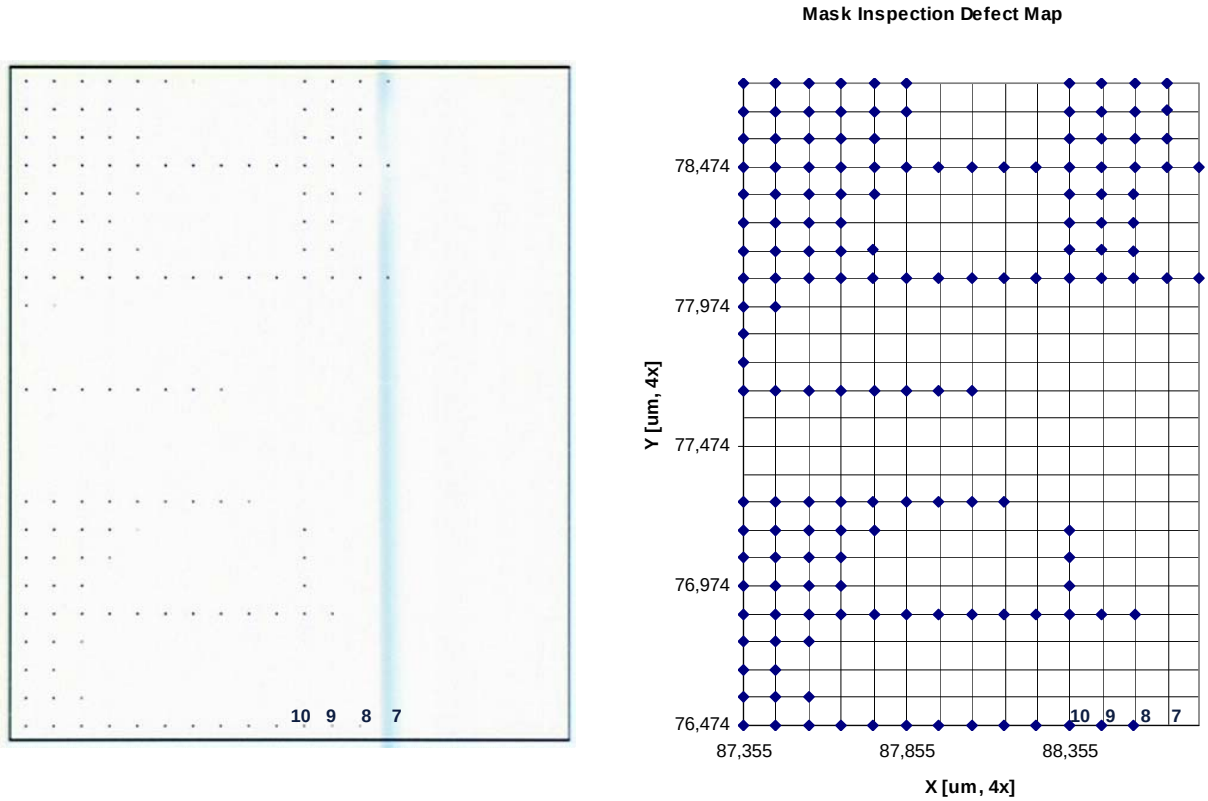

Figure 13. Optical microscope image of Wafer exposed with alt. PSM programmed defect testmask and disar illumination. (10x, Dark Field, Microscope image is inverted for better printing).

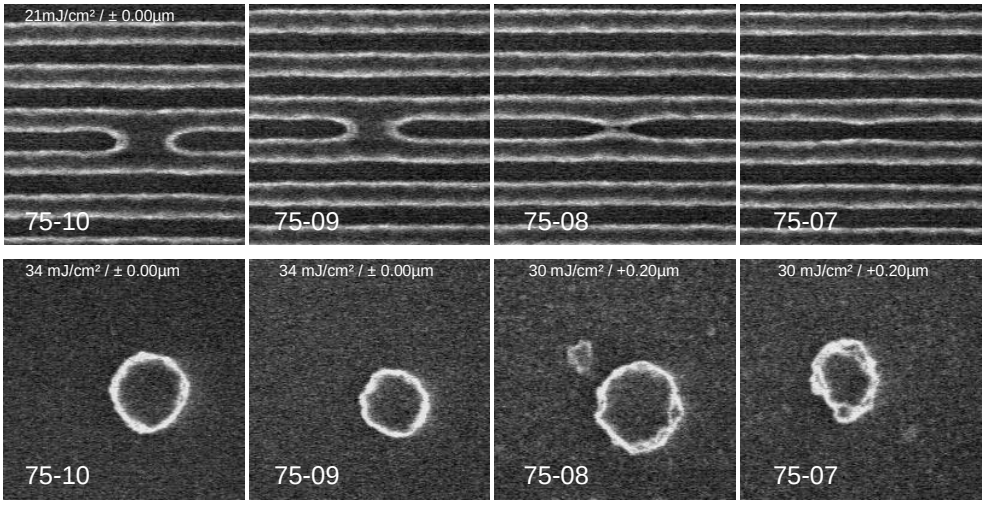

Figure 14. Wafer printing studies of Qz. bridging defects, (top) at nominal circular illumination and (bottom) at disar illumination.

3. CONCLUSION

From the simulation and experimental results we can conclude that the technique of complementary illumination is a simple but efficient method of assessing defect images in dense array structures. For mask repair it allows to automatically find and classify repaired defect sites. In the absence of a defect, the background intensity is a measure for the line-space duty cycle. Its standard deviation is a measure for the jitter from mask writing and fracturing. Finally, we demonstrated the application for finding defects by wafer printing. Using dipole illumination for alt. PSM, most errors can already be found with the darkfield setting of an optical microscope. As the technique is independent of the actual mask technology used, this application is interesting to provide a baseline inspection capability in the dense array for novel mask technologies for which no established mask inspection solution is available at the moment.

ACKNOWLEDGMENTS

The authors would like to thank Jan Heumann for the inspection results, and for the fruitful discussion with Alexander Seidl, Jörg Thiele and Christoph Nölscher.

REFERENCES

1. N. Shiraishi, S. Hirukawa, Y. Takeuchi, N. Magome, “New imaging technique for 64M-DRAM,” Proc. SPIE 1674, Optical/Laser Microlithography, pp. 741, 1992.
2. J. S. Petersen, “Optical proximity strategies for desensitizing lens aberrations,” *Proc. SPIE* **4404**, *Lithography for Semiconductor Manufacturing II*, pp. 254-265, 2001.
3. M. D. Levinson, N. S. Viswanathan, R. A. Simpson, “Improving Resolution with a Phase-Shifting Mask,” *IEEE Trans. Elect. Dev.* **ED-29**, pp. 1828-1836, 1982.
4. O. Nozawa, Y. Shiota, H. Mitsui, T. Suzuki, Y. Ohkubo, M. Ushida, S. Yusa, T. Nishimura, K. Noguchi, S. Sasaki, H. Mohri, N. Hayashi, “Development of attenuating PSM shifter for F2 and high-transmission ArF lithography,” *Proc. SPIE* **5130**, *Photomask and Next-Generation Lithography Mask Technology X*, pp. 39-50, 2003.
5. W. Dettmann, J. P. Heumann, T. Hagner, R. Koehle, S. Rahn, M. Verbeek, M. Zarrabian, J. Weckesser, M. Hennig, N. Morgana, “Qualification of alternating PSM: defect inspection analysis in comparison to wafer printing results,” *Proc. SPIE* **5130**, *Photomask and Next-Generation Lithography Mask Technology*, p. 415, 2003.
6. R. Koehle, W. Dettmann, M. Verbeek, “Fourier analysis of AIMS images for mask characterization,” *Proc. SPIE* **5130**, *Photomask and Next-Generation Lithography Mask Technology*, p. 545, 2003.
7. A. Wong and A. Neureuther, “Mask topography effects in projection printing of phase-shifting masks,” *IEEE Transactions on Electron Devices* **41**, pp. 895-902, June 1994.
8. U. A. Griesinger, L. Mader, A. Semmler, W. Dettmann, C. Noelscher, R. Pforr, “Balancing of alternating phase-shifting masks for practical application: modeling and experimental verification,” *Proc. SPIE* **4186**, *20th Annual BACUS Symposium on Photomask Technology*, pp. 372-383, 2001.
9. A. M. Zibold, R. Schmid, K. Boehm, R. Birkner, “Aerial image measuring system at 193 nm: a tool-to-tool comparison and global CD mapping,” *Proc. SPIE* **5567**, *24th Annual BACUS Symposium on Photomask Technology*, pp. 1083-1090, 2004.
10. S. Akima, T. Komizo, S. Kawakita, Y. Kodera, T. Narita, K. Ishikawa. “Phase defect printability and mask inspection capability of 65-nm technology node Alt-PSM for ArF lithography,” *Proc. SPIE* **5567**, *24th Annual BACUS Symposium on Photomask Technology*, pp. 23-35, 2004.
11. D. H. Chung, K. Ohira, N. Yoshioka, K. Matsumura, T. Tojo, M. Otaki, “Optical Mask inspection Strategy for 65nm node and beyond,” *Proc. SPIE* **5567**, *24th Annual BACUS Symposium on Photomask Technology*, pp. 320-329, 2004.